Acta metall. mater. Vol. 38, No. 7, pp. 1279–1290, 1990
Printed in Great Britain.

0956-7151/90 $3.00 + 0.00

EXPERIMENTAL DETERMINATION OF INTERFACIAL TOUGHNESS CURVES USING BRAZIL-NUT-SANDWICHES

J.-S. WANG[1]† and Z. SUO[2]

[1]Division of Applied Sciences, Harvard University, Cambridge, MA 02138, U.S.A. and
[2]Mechanical Engineering Department, University of California, Santa Barbara, CA 93106, U.S.A.

(*Received* 27 *November* 1989)

Abstract—A Brazil-nut-sandwich with a crack on a substrate/interlayer interface is developed for fracture testing. The fracture loading phase is controlled by the angle of diametral compression. Interfacial fracture mechanics is summarized and adopted in reporting data. Experiments are conducted with aluminum, brass, steel and plexiglass as substrates and epoxy as interlayer. Interfacial toughness curves are measured for large range of loading phase. Effects of the roughness of the surfaces prior to bonding on the interfacial toughness are demonstrated. Failure patterns for the adhesive structure under different loading modes are observed with a scanning electron microscope. For the metal/epoxy systems, when the remote loading is predominantly mode I, cracks tend to kink out of interfaces and run within the epoxy layer, although the bulk epoxy fracture energy is much higher than the interfacial toughness. At large loading phases, abnormally high apparent toughness is measured. These observations are discussed in the light of crack path selectiom criteria in adhesive joints and large scale contact zone of crack faces.

Résumé—Un sandwich avec une fissure à l'interface substrat-intercouche est mis au point pour des essais de rupture. La charge de rupture est contrôlée par l'angle de compression diamétrale. La mécanique de la rupture interfaciale est résumée et adoptée pour l'interprétation des résultats. Des expériences sont effectuées sur des substrats d'aluminium, de laiton, d'acier et de plexiglass, avec de l'époxy comme intercouche. Les courbes de tenacité interfaciale sont mesurées pour de large gammes de charge. Les effets de la rugosité des surfaces avant liaison sur la tenacité interfaciale sont mis en évidence. Par microscopie électronique à balayage on observe des exemples d'échec de la structure adhésive sous différents modes de charge. Pour les systèmes métal/époxy, lorsque le chargement à distance est principalement du mode I, les fissures tendent à s'écarter des interfaces et de passer à l'intérieur de la couche d'époxy bien que l'énergie de rupture de l'époxy massive soit beaucoup plus élevée que la ténacité interfaciale. Pour de grandes charges, on mesure une ténacité apparente anormalement élevée. Ces observations sont discutées à la lumière des critères de sélection du trajet des fissures dans les joints adhésifs et dans la zone de contact à grande échelle des lèvres de la fissure.

Zusammenfassung—Für Bruchversuche wird eine brasilnußartige Schichtstruktur mit einem Riß an der Grenzfläche zwischen Substrat und Zwischenschicht entwikelt. Die Bruchbelastung wird über den Winkel der diametralen Kompression eingestellt ('Phase'). Die Bruchmechanik an der Grenzfläche wird zusammengefaßt und mit vorgelegten Daten belegt. Experimente werden an Aluminium, Messing, Stahl und Plexiglas als Substrate und einem Epoxidkleber als Zwischenschicht durchgeführt. Die Kurven der Grenzflächenzähigkeit werden in einem großen Bereich der Belastungsphase gemessen. Einflüsse der Rauhigkeit der Oberflächen vor der Verklebung auf diese Zähigkeit werden aufgezeigt. Die Erscheinungsbilder des Bruches werden unter verschiedenen Belastungsarten in einem Rasterelektronenmikroskop beobachtet. Bei den Metall-Kleber-Systemen neigen die Risse bei Belastung entsprechend Mode I zum Ausbrechen aus der Grenzfläche in die Kleberschicht, obwohl die Bruchenergie im Volumen des Epoxidklebers viel größer ist als die Grenzflächenzähigkeit. Bei großen Belastungsphasen wird eine abnorm hohe effektive Zähigkeit gemessen. Diese Beobachtungen werden anhand von Auswahlkriterien für den Rißweg in Klebeverbindungen und in großen Kontaktbereichen von Bruchflächen diskutiert.

1. INTRODUCTION

For ceramic/ceramic fiber reinforced composite materials, moderately "weak" bonding of matrix/fiber interfaces, allowing debonding and fiber pull-out, enhances the overall toughness. On the other hand, a "strong" bonding between layers of different solids is usually a prerequisite for routine performance for microelectronic devices. Quantification of interfacial fracture resistance has emerged to be a key to understanding these heterogeneous systems.

The purpose of the *interfacial fracture mechanics* is to define a measurable and usable material property, *toughness*, to parameterize fracture resistance of interfaces. A comprehensive mechanics scheme, at least for brittle interfacial failures, has been established recently, including extraction of toughness from mechanical testing raw data and application of the measured toughness in material and structural design. The rapid development of this scheme is manifested in part by many review articles published in the last few years [1–6]. The basic notions will be put into perspective in Section 2.

†Present address: Max-Planck Institut fur Eisenforschung, 4000 Dusseldorf, F.R.G.

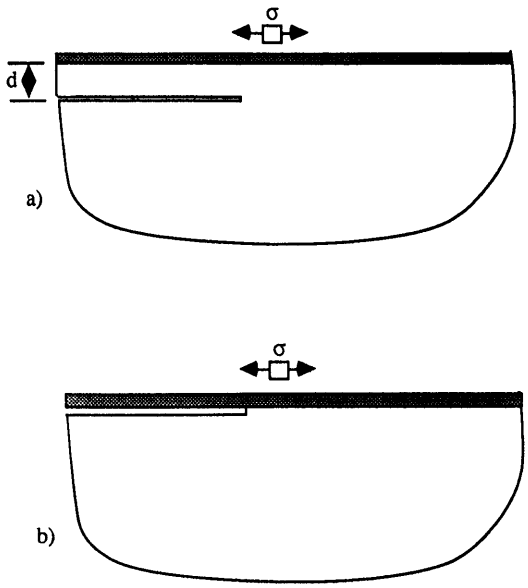

Fig. 1. Examples to contrast two situations: (a) crack in a homogeneous material and, (b) an interfacial crack.

From mechanics point of view, a difference between cracking in a monolithic solid and cracking on an interface is that the former usually seeks a trajectory with opening mode (mode I) locally, while the latter is confined on the interface regardless of local stress mode provided the interface is weak. Depicted in Fig. 1 are examples to contrast the two situations. Consider a thin elastic film deposited on an elastic substrate, and the processing route is such that a significant residual tensile stress develops in the film. If the film/substrate bonding is strong and the substrate is brittle, the crack will divert into the substrate and attain a trajectory parallel to the interface [Fig. 1(a)]. The steady-state depth d measured experimentally is consistent with the calculated value under the hypothesis that $K_{II} = 0$ [7, 8]. An implication of this path selection criterion is that one needs only one material property, fracture toughness K_{Ic} (of the substrate in the present case), to tell how brittle a monolithic solid is. If the interface is poorly bonded, however, the crack will stay on the interface regardless of the relative proportion of the opening and shearing loads [Fig. 1(b)]. Indeed, for this situation analysis [9] shows that the opening and shearing modes are comparable in magnitude. The relevant material information now is the fracture toughness at the specified loading phase.

Experimental data on glass/epoxy interface indicate that interfacial toughness can be a strong function of loading phase [10]. Micro-mechanical models have been proposed to understand the trend of toughness curves [11]. Yet it is premature at this stage to rely on those models to predict phenomenological functional forms of toughness curves. The aim of the present work is to develop an experimental method that allows continuous measurement of interfacial toughness as a function of loading phase, so as to enlarge experimental data base for future modelings or applications.

The fracture specimen we propose is Brazil-nut-sandwiches illustrated in Fig. 2. Loading phase is controlled by the compression angle θ. The homogeneous base specimen absent of the interlayer is mode I when $\theta = 0°$ and is mode II when $\theta \approx 25°$. A sandwich is made using epoxy to glue two identical halves. The substrates were of steel, brass, aluminum and plexiglass. The elastic constants are given in Table 1. The materials selected are easy to handle and allow us to generate sizable amount of toughness data at low cost. We believe such a sandwich set-up can be used for metal/ceramic systems and many others as well.

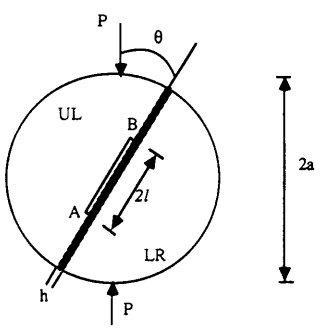

Fig. 2. A Brazil-nut-sandwich in diametral compression.

Table 1. Elastic constants

Material	Shear modulus (GPa)	Poisson's ratio
Aluminum	26	0.35
Brass	48	0.34
Steel	84	0.28
Plexiglass	1.1	0.35
Epoxy	1.5	0.34

2. BASICS OF INTERFACIAL FRACTURE MECHANICS

In this section we summarize interfacial fracture mechanics in the context of mechanical testing. The precise definition of the *loading phase*, as well as the *interfacial toughness* at a specific loading phase will be given. We will emphasize the underlying assumptions as well as the key limitations of the present framework at the end of the section.

2.1. Interfacial toughness curve $G_c(\hat{\psi})$

Figure 3 gives the generic configuration of an interface crack. Solid 1 is above the interface and solid 2 is below. Both are taken to be linearly elastic, homogeneous and isotropic, with shear moduli μ_1 and μ_2, Poisson's ratios υ_1 and υ_2, respectively. Plane strain deformation is assumed. The stress field depends on two Dundurs elastic mismatch parameters [12]

$$\alpha = \frac{(1-\upsilon_2)/\mu_2 - (1-\upsilon_1)/\mu_1}{(1-\upsilon_2)/\mu_2 + (1-\upsilon_1)/\mu_1},$$

$$\beta = \frac{1}{2}\frac{(1-2\upsilon_2)/\mu_2 - (1-2\upsilon_1)/\mu_1}{(1-\upsilon_2)/\mu_2 + (1-\upsilon_1)/\mu_1}. \quad (1)$$

Two other useful combinations are related to the Dundurs' parameters as

$$\frac{\bar{E}_1}{\bar{E}_2} = \frac{1+\alpha}{1-\alpha}, \quad \epsilon = \frac{1}{2\pi}\ln\frac{1-\beta}{1+\beta}. \quad (2)$$

Here $\bar{E} = 2\mu/(1-\upsilon)$ is the plane strain tensile modulus, and ϵ is the oscillatory index responsible for various pathological behaviors in linear elasticity solutions for interfacial cracks. The elastic mismatch parameters are given in Table 2. The convention that substrate is solid 1 and interlayer is solid 2 is taken throughout this work.

Let (r, ϕ) be the polar coordinate centered at the crack tip. As r approaches the tip the Williams asymptotic stress field [13] can be written as

$$\sigma_{ij}(r,\phi) = \frac{\mathrm{Re}[Kr^{i\epsilon}]}{\sqrt{2\pi r}}\tilde{\sigma}^{\mathrm{I}}_{ij}(\phi) + \frac{\mathrm{Im}[Kr^{i\epsilon}]}{\sqrt{2\pi r}}\tilde{\sigma}^{\mathrm{II}}_{ij}(\phi) \quad (3)$$

The complex quantity K, referred to as the interfacial stress intensity factor, measures the *amplitude* and *phase* of the external loading. The dimensionless angular distributions $\tilde{\sigma}^{\mathrm{I}}_{ij}$ and $\tilde{\sigma}^{\mathrm{II}}_{ij}$ can be found in [5].

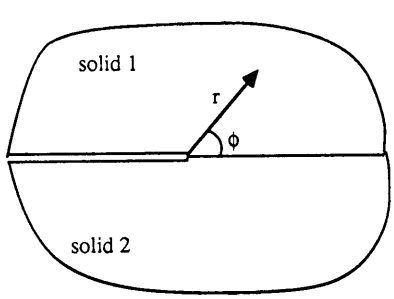

Fig. 3. Conventions of an interfacial crack.

Table 2. Elastic mismatch parameters

Bimaterial	α	β	ϵ
Aluminum/epoxy	0.90	0.218	−0.071
Brass/epoxy	0.94	0.228	−0.074
Steel/epoxy	0.96	0.232	−0.075
Plexiglass/epoxy	−0.15	−0.029	0.009

They are normalized such that the interface traction ($\phi = 0$) is given by

$$\sigma_{yy} + i\sigma_{xy} = Kr^{i\epsilon}/\sqrt{2\pi r}. \quad (4)$$

This equation may be taken as the defining equation of K. Between the crack faces the displacement jumps

$$\delta_y + i\delta_x = \frac{8Kr^{i\epsilon}}{E^*(1+2i\epsilon)\cosh\pi\epsilon}\sqrt{\frac{r}{2\pi}}. \quad (5)$$

Here E^* is an average modulus defined by

$$\frac{2}{E^*} = \frac{1}{\bar{E}_1} + \frac{1}{\bar{E}_2}. \quad (6)$$

Note $r^{i\epsilon} \equiv e^{i\epsilon\ln r} = \cos(\epsilon\ln r) + i\sin(\epsilon\ln r)$, stress oscillation and crack faces interpenetration are implied by Williams solution as r approaches the tip.

The interfacial fracture mechanics is established by correlating K in different specimens of the same bimaterial interface. However, as a consequence of the peculiar singularity, K has funny, material dependent dimensions, and the ratio of the shear and normal components of the interface traction is not well-defined as r approaches the tip. One can not talk about *fracture mode* in the same sense as in the fracture mechanics for homogeneous solids. A remedy, as suggested in [1], is to appeal to a fixed length $\hat{L}$, and use the combination $K\hat{L}^{i\epsilon}$ as the basic parameter. The latter combination has the dimension of conventional stress intensity factors. It has been proposed to define the *loading phase* $\hat{\psi}$ as

$$K\hat{L}^{i\epsilon} = |K|e^{i\hat{\psi}}. \quad (7)$$

Note that $|\hat{L}^{i\epsilon}| = 1$ and $|K\hat{L}^{i\epsilon}| = |K|$, $\hat{\psi}$ is indeed the phase angle of the complex quantity $K\hat{L}^{i\epsilon}$. It does not matter one chooses $\hat{L}$ as 1 μm, 0.1 mm, or 5 cm, so long as one chooses a fixed length in reporting data.

Instead of $|K|$, a physically more appealing quantity to describe the *loading amplitude* is the energy released G for a unit area of an interface to decohere, which is equivalent to $|K|$ with an Irwin-type relation

$$G = \frac{|K|^2}{E^*\cosh^2\pi\epsilon}. \quad (8)$$

Having defined both loading phase and amplitude, one can define the *interfacial toughness curves* precisely. At a prescribed loading phase $\hat{\psi}$, the maximum loading amplitude G that an interface can sustain without decohesion is called the toughness of the interface at this phase, noted as $G_c(\hat{\psi})$.

We emphasize that the fixed length $\hat{L}$ associated with $\hat{\psi}$ should also be *explicitly* reported, since it affects the meaning of $\hat{\psi}$. For example, if two different

lengths $\hat{L}_1$ and $\hat{L}_2$ are used to plot the same interfacial toughness curve, a translation in the $\hat{\psi}$-coordinate incurs

$$\hat{\psi}_2 - \hat{\psi}_1 = \epsilon \ln(\hat{L}_2/\hat{L}_1). \tag{9}$$

Obviously the loading phase so defined has no absolute physical significance, it is only a relative measure of loading mode. For example, it is *not* correct in general to associate $\hat{\psi} = 0$ with opening mode, because an interface crack contains the intrinsic mode mixity. What is the range of the loading phase in which the toughness can be validity measured? We will answer this in Section 5.2 in the context of small scale contact.

The present work develops an experimental technique to determine toughness curves for several interfaces (aluminum/epoxy, brass/epoxy, steel/epoxy and plexiglass/epoxy). The measured curves are plotted in Fig. 7. As indicated on each plot, $\hat{L} = 0.1$ mm is chosen in defining loading phase $\hat{\psi}$. The experimental details will be given in Section 4, and here we shall continue the discussion on the general aspects of interfacial fracture mechanics.

2.2. K-calibration

For a given bimaterial structure with an interfacial crack, K takes the form

$$K = YT\sqrt{L}\,\hat{L}^{-i\epsilon}e^{i\psi} \tag{10}$$

where T is a representative amplitude of the stress to load the structure, L a characteristic length, Y a dimensionless real positive number, and ψ by definition the phase angle of $KL^{i\epsilon}$. Both Y and ψ depend on the geometric and loading details of the structure, and to obtain them for a given structure usually requires one to solve a non-trivial elasticity problem. A relation of form (10) connecting the applied load and K is called a *K-calibration* for the structure. Catalogs of K-calibrations for several interfacial fracture specimens are available in [5, 6].

With a K-calibration (10) for a given specimen, the loading amplitude G can be calculated from (8), and the loading phase is calibrated by

$$\hat{\psi} = \psi + \epsilon \ln(\hat{L}/L) \tag{11}$$

which is obtained by comparing (10) with (7). In equation (11) L is the specimen size used in the K-calibration, and $\hat{L}$ is the fixed length independent of specimens that one has chosen in defining the loading phase $\hat{\psi}$.

2.3. K-Annulus and small scale irregularities

In the above formulation, each solid is assumed to be homogeneous and linearly elastic, the interface is thought to be a smooth two-dimensional object without thickness, and the crack faces are taken to be traction-free. These requirements can never be accurately satisfied in reality. In addition, for any given structure the crack tip field must be perturbed by its external geometry and loading distribution. These considerations lead to the notion of K-annulus. If the size of all *irregularities* (grains, voids, inelastic zones, contact zones, interface thickness and roughness, craze or fiber bridging zones, etc.) is small compared with the smallest length of the specimen, owing to the square root singularity, the Williams field is still approximately unperturbed in an *annulus* larger than the irregularity size but smaller than the external geometry. Within such an annulus the stress field is completely parameterized by K. Any other more detailed information on both the external specimen geometry and near-tip irregularities is lost in the annulus. The notion of K-annulus, together with the Williams solution, is the backbone of the fracture mechanics methodology. For historical reasons two irregularities, inelastic deformation and crack face contact, have captured much attention. Their implications to fracture testing will be summarized in Section 5.

3. BRAZIL-NUT-SANDWICHES

3.1. Calibration of the homogeneous base specimen

We use Brazil-nut as a base specimen, which is a homogeneous circular disk of radius a, with a center crack of length $2l$ (as illustrated in Fig. 2 but without the interlayer). The homogeneous specimen has been used for brittle solids for many years. Readers are referred to [14, 15] for the recent bibliography. The loading phase of the homogeneous specimen is controlled by the compression angle, θ: the specimen is mode I when $\theta = 0°$, and mode II when $\theta \approx 25°$. More precisely, the conventional stress intensity factors are

$$K_{\mathrm{I}} = f_{\mathrm{I}} P a^{-1/2}, \quad K_{\mathrm{II}} = \pm f_{\mathrm{II}} P a^{-1/2} \tag{12}$$

where the plus sign is for tip A and the minus for tip B. The nondimensional calibration factors f_{I} and f_{II} are functions of the compression angle θ and relative crack size l/a, and available in fitting polynomial forms in [14].

The energy release rate can be calculated from

$$G = \frac{1}{\bar{E}_1}(K_{\mathrm{I}}^2 + K_{\mathrm{II}}^2) = (f_{\mathrm{I}}^2 + f_{\mathrm{II}}^2)\frac{P^2}{\bar{E}_1 a}. \tag{13}$$

The loading phases at tip A and B are

$$\tan^{-1}(K_{\mathrm{II}}/K_{\mathrm{I}}) = \pm \tan^{-1}(f_{\mathrm{II}}/f_{\mathrm{I}}). \tag{14}$$

respectively. Equations (13) and (14) are plotted in Fig. 4 using the basic solution in [14]. These curves were used in converting the measured critical loads and compression angles to points on toughness curves.

3.2. Sandwiched Brazil nuts

Any homogeneous base specimen can be converted to an interfacial fracture specimen by sandwiching a thin layer of a second material. The general setup is analyzed in [16]. Here we sandwich the Brazil nut of radius a, with an epoxy layer of thickness h and a

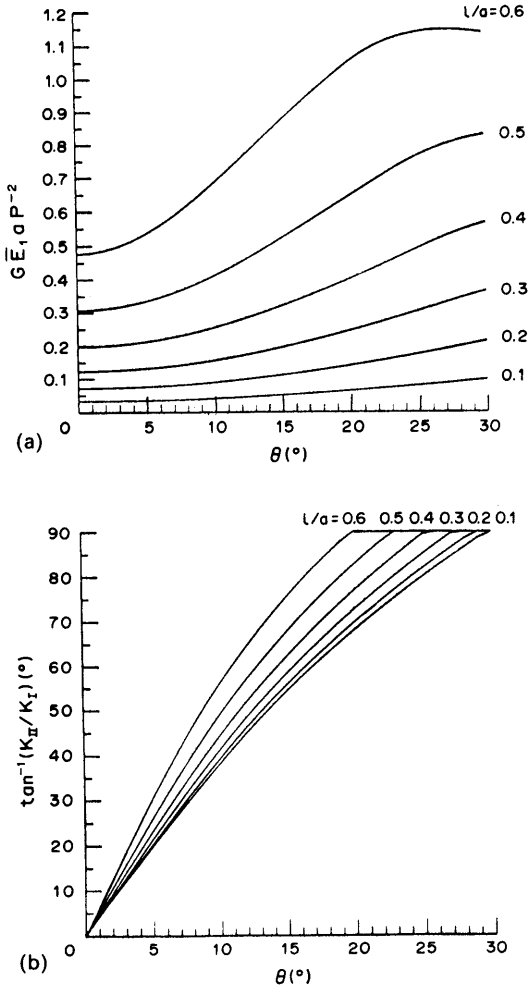

Fig. 4. Homogeneous Brazil-nut calibrations: (a) the normalized energy release rate and, (b) the loading phase.

crack of size $2l$ on one of the substrate/interlayer interfaces (Fig. 2).

A remarkable feature common to all thin-layer-sandwiches is that the residual stress in the layer does *not* drive the crack, because the strain energy stored in the layer due to residual stress is not released in the process of cracking. Thus, one does not have to measure the residual stress to obtain toughness. On the other hand, excessive residual stress may invalidate the basis for the correlation of the interfacial toughness. The Williams asymptotic stress field (3) on which the fracture mechanics is built is the approximate stress state in the K-annulus only when the higher order terms are not excessively large. For example, suppose the measured $|K| = 0.3$ MPa m$^{1/2}$, and the process zone size $r = 0.01\ \mu$m. From equation (4), the magnitude of the stress induced by K is about $\sigma \approx 1.2$ GPa. The residual stress developed in many bonding processes may exceed this value for metal/ceramic or ceramic/ceramic systems. The K-field may therefore lose its physical significance and toughness data obtained this fashion should be used with caution. This is not of concern for the present system since the residual stress is typically very small.

When h is much smaller than other in plane macroscopic length scale, the energy release rate can still be calculated from equation (13), as if the specimen were made only of substrate material. This is true because of the conservation of the J-integral and because the introduction of the thin layer does not perturb the remote K field.

The interfacial loading phases at tips A and B are shifted from those for the homogeneous specimen according to

$$\hat{\psi} = \pm \tan^{-1}(f_{II}/f_I) + \omega + \epsilon \ln(\hat{L}/h) \qquad (15)$$

respectively. Here ω, tabulated in [16], is the shift due to substrate/interlayer mismatch of elastic constants, and the last term is the shift due to ϵ and re-scaling in the context of (11).

By measuring the critical load P and the compression angle θ, and by specifying a length $\hat{L}$, one can calculate G_c and $\hat{\psi}$ according to the above formulae.

According to [16], $\omega \approx -13°$ for all three metal/epoxy systems, and $\omega \approx 1°$ for the plexiglass/epoxy system. We chose $\hat{L} = 100\ \mu$m, and measured $h = 80$–$300\ \mu$m. For metal/epoxy systems, the total shift is $-14°$ to $-8°$. Almost no shift is needed for plexiglass/epoxy system, because the elastic properties are similar for the two materials.

4. EXPERIMENTAL RESULTS

4.1. Specimen preparation and testing

Half-circular disks were made of 420 stainless steel, 1090 aluminum, C27000 brass and commercial plexiglass, with radius $a = 12.7$ mm and thickness 6.35 mm. Both as-machinery-milled surfaces and mechanically-polished surfaces using $0.05\ \mu$m alumina powder were prepared to study the effect of surface roughness prior to bonding on interfacial toughness. The bonding surfaces before and after polishing are shown in Fig. 5. Two identical halves were joined by epoxy as follows. (1) Clean the substrates carefully with organic solvents and an ultrasonic cleaner. (2) Smear a very thin film of solid paraffin on the center area of the joining edge of one substrate and epoxy jell on the whole edge of the other substrate. (3) Press the two halves together with certain compression to control the thickness of the epoxy jell. (4) Let epoxy set for about 24 h. Since epoxy did not wet paraffin, the paraffin smeared area was taken to be a sharp pre-existing crack. The relative crack size (l/a) was controlled to be 0.25 ± 0.03. The thickness of epoxy layers were measured with an optical microscope, ranging 80–$300\ \mu$m. They were thin enough to allow us to use the calibration in Section 3, yet not too thin to interfere with the microirregularities.

Diametral compression tests were conducted at room temperature with an electromechanical Instron machine. The compression angle θ was measured with the deviation of $\pm 0.5°$. Figure 6

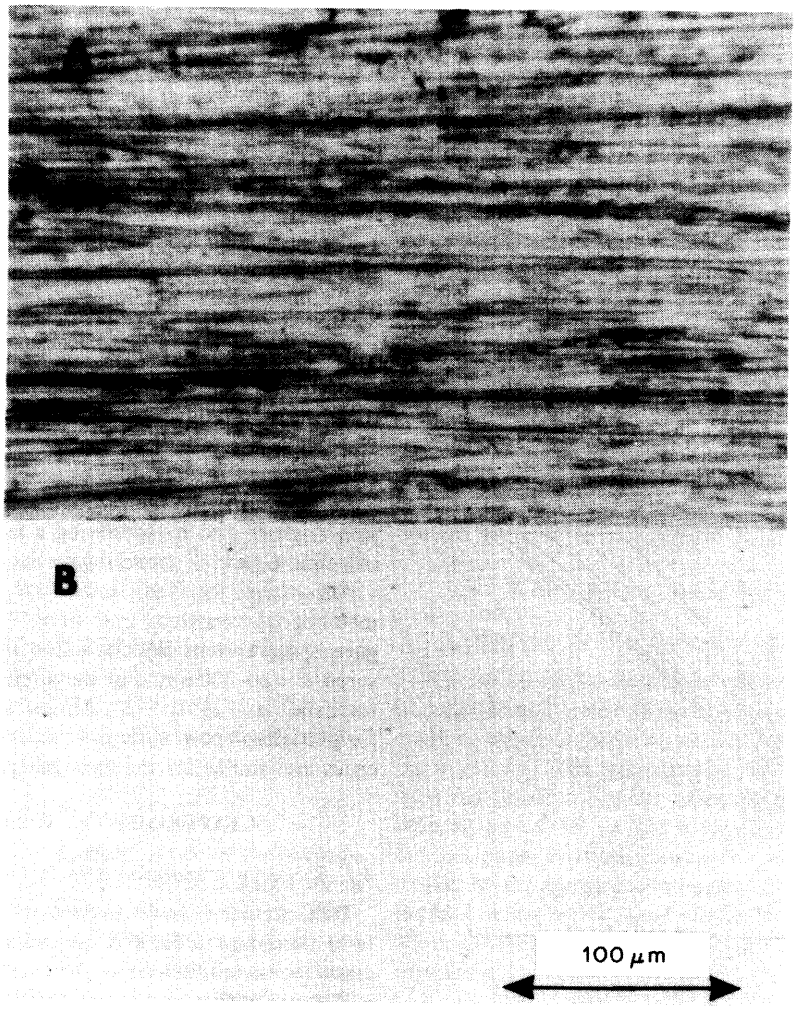

Fig. 5. Surfaces prior to bonding: (a) as-milled and (b) mechanically polished.

shows a typical load–displacement curve. The disk deformed linearly until it broke into halves catastrophically. No plastic deformation was detected and cracks propagated dynamically. Most separated halves were recycled by dissolving epoxy residue. About 160 tests were run.

The peak load P_c at the onset of failure was converted to fracture toughness G_c by (13). There is some ambiguity in determining the loading phase ψ from (15), since we usually do not know which tip starts to run first. In the calculation we took tip A to run first. The choice is somewhat arbitrary. A (weak) justification for this choice is that the magnitude of the loading phase is usually smaller at tip A than B, and it is believed that toughness is smaller at lower loading phase. A modified specimen avoiding this ambiguity will be proposed at the end of the section.

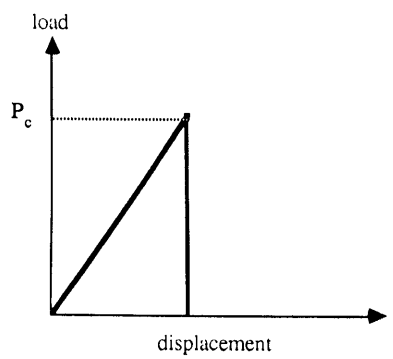

Fig. 6. A load–displacement curve.

The measured interfacial toughness curves are plotted in Fig. 7. Observe that the interfacial toughness G_c varies with the loading phase ψ. It is meaningless to talk about the interfacial toughness unless one specifies the loading phase. Also shown in Fig. 7 is the effect of surface polishing prior to bonding. For the aluminum/epoxy and brass/epoxy systems, polished surfaces enhanced the toughness within large range of loading phase. For the steel/epoxy system, however, the effect is not so pronounced.

The solid circles in the plots are abnormally high. Microscopic observations (Section 4.2) revealed that they corresponded to fracture within the epoxy layer instead of along the interfaces. The theoretical

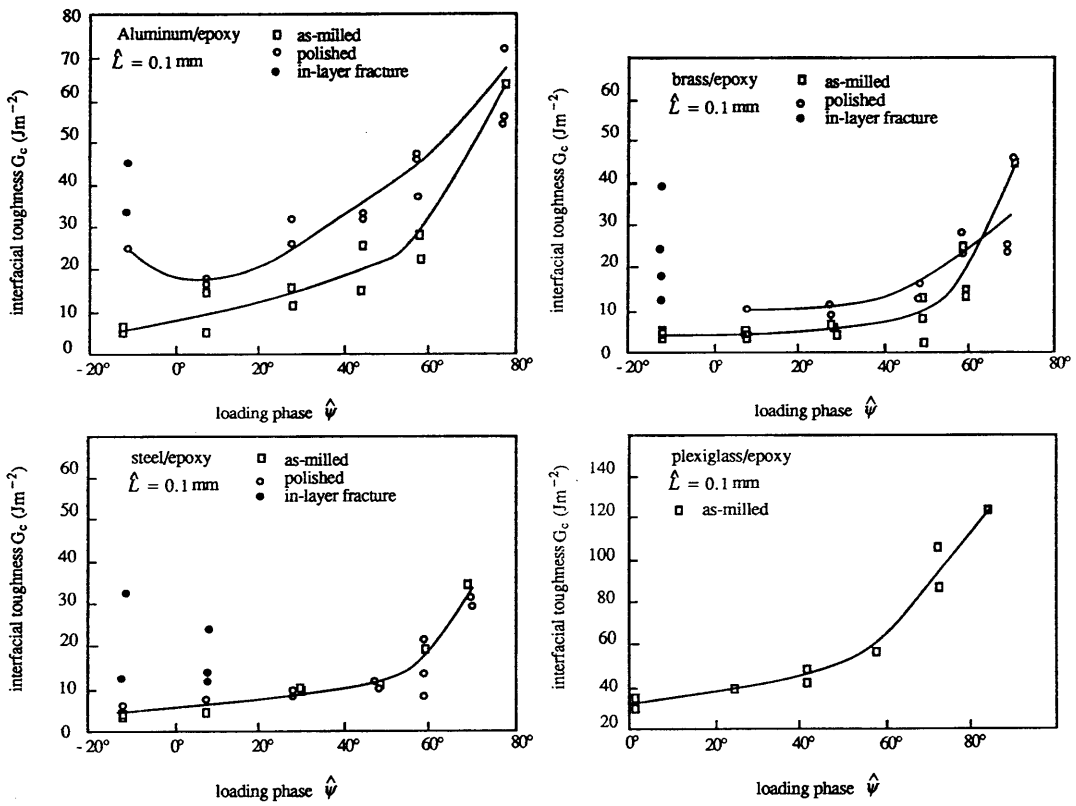

Fig. 7. The toughness curves for several model interfaces.

explanations will be detailed in Section 5.4. Also noticed is that, for all the metal/epoxy systems, the apparent toughness values in the range $\hat{\psi} > 60°$ are quite high compared with the trend set by the toughness at lower loading phases. We suspect this was caused by large-scale-contact between crack faces resulting from the oscillatory intex ϵ, as will be discussed in Section 5.2. By contrast, the toughness curve for the plexiglass/epoxy system does not seem to show such a dramatic rising, which is consistent with the fact that the two solids are elastically similar and have a small value of ϵ, see Table 2.

4.2. Observation of fracture patterns

Fracture surfaces were mounted and photographed in a scanning electron microscope. We distinguished five failure types, which are illustrated in Fig. 8 schematically.

When the loading phase is large, most our specimens failed by the first type: the interface containing the pre-existing crack decohered, leaving an unbroken epoxy layer on the other substrate. This is the most desired situation for the purpose of measuring interfacial toughness.

For type 2 failure, debonding started at tip *A* and ran on the pre-existing crack plane, leaving the epoxy layer on the LR half. At tip *B* the crack ran along the interface for a short distance, and then kinked to the other interface, leaving a portion of the epoxy layer on the UL half. Such a kinking is shown in Fig. 9.

Figure 10 shows the situation where both crack tips kinked (type 3).

As opposed to type 2, kinking occurred at tip *A* but not at tip *B* in type 4.

Type 5 failure happened when substrates were metals and the remote loading is predominantly mode I ($\theta = 0$). In this situation the crack kinked out of the interface and ran *into* the epoxy layer parallel to the interfaces, leaving epoxy residues on both substrates. Also observed are patches of metal surfaces on both sides where epoxy was peeled off. Figure 11 shows a mated pair of fracture surfaces. Interlayer fractographs at various magnifications are shown in Fig. 12.

Observe that the fracture energy for bulk epoxy is in the range 50–200 J m^{-2}, which is much higher than the metal/epoxy interfacial toughness at low loading phases. Kinking into epoxy is energetically unfavorable. Similarly the in-layer crack path has higher fracture resistance than interfacial crack. Theoretical explanations for these abnormal observations will be discussed in the next section. Such phenomena may be termed as trapping of cracks onto energetically unfavorable paths, which seem to result from the substantial elastic mismatch in metal/epoxy adhesive joints. By contrast, we never found in-layer fracture in the plexiglass/epoxy system, where elastic moduli of the two materials are similar. We did find occasionally, however, that crack kinked to join the opposite interface in the plexiglass/epoxy systems.

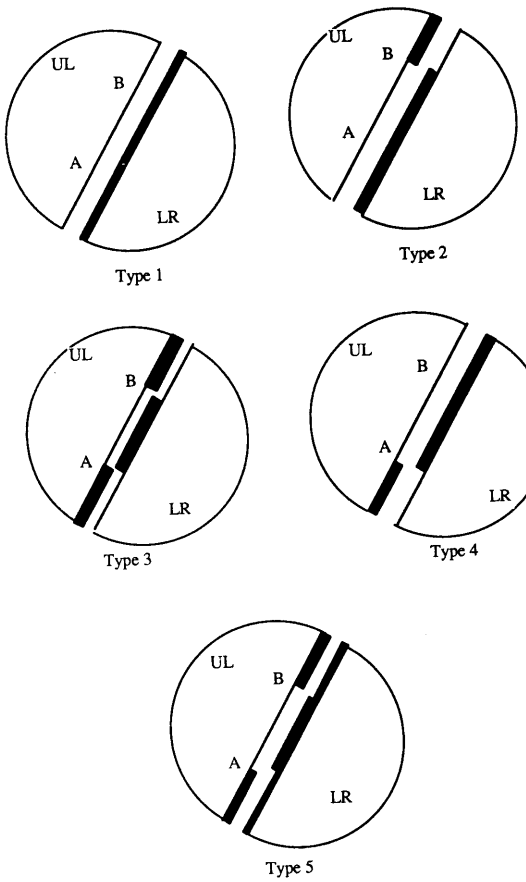

Fig. 8. Five failure types.

4.3. *A modified Brazil-nut-sandwich*

We propose to modify the specimen by introducing a non-coplanary pre-existing crack, as illustrated in Fig. 13. The arrangement is symmetric in the sense that every detail is recovered after an 180° in-plane rotation. A corollary is that the loading phases, as well as the loading amplitudes at the two tips are identical, and equal that of tip A of the old specimen [equation (15)]. With this modified sandwich, one does not encounter the ambiguity in calibrating the loading phase discussed in Section 4.1. Further, one can extend the loading phase to span nearly 180° by allowing the compression angle to be negative.

5. THEORETICAL CONSIDERATIONS

A number of theoretical considerations are grouped in this section to account for the observed fracture patterns, as well as to justify the validity of the measured interfacial toughness curves.

5.1. *Small scale yielding*

In the context of small scale irregularities discussed in Section 2.3, the requirement of small scale yielding sets an upper bound to the toughness that can be measured validly with a given specimen. For an isolated interfacial crack tip, the size of the plastic zone around the tip is given by [3]

$$r_p = \Lambda \frac{|K|^2}{\sigma_0^2} \tag{16}$$

where K is the complex stress intensity factor, σ_0 is the smaller of the yield stresses of the two solids, and the dimensionless number Λ, ranging from 0.1 to 0.6, is a function of loading phase and also depends weakly on the details of material properties. Small scale yielding requires r_p to be much less than the representative specimen size: larger specimens are needed to test tougher interfaces.

With Brazil-nut-sandwiches, the smallest specimen size is the interlayer thickness h, and the relevant yield stress is that for epoxy, taken to be $\sigma_0 = 85$ MPa. With the measured interfacial toughness G_c in Fig. 7, one can calculate from (8) that $|K|_c = 0.3$–0.7 MPa m$^{1/2}$. The plastic zone size is thus estimated

Fig. 9. The fracture surface of a UL substrate. The pre-existing crack initially ran along the paraffin smeared interface, and then kinked and the debonding proceeded along the other interface.

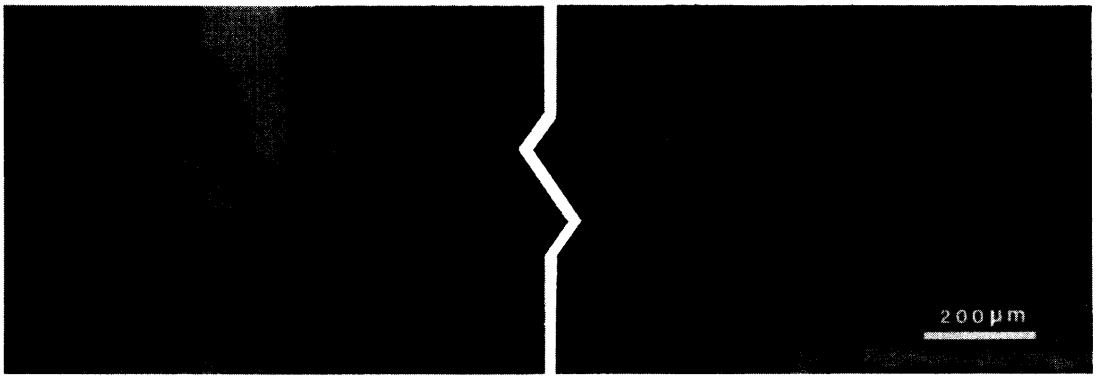

Fig. 10. The fracture surface of a UL substrate. Both crack tips kinked to the opposite interface. The center portion is paraffin smeared which we took to be pre-existing crack. The brighter patches are the substrate surface, and the darker ones are epoxy residues.

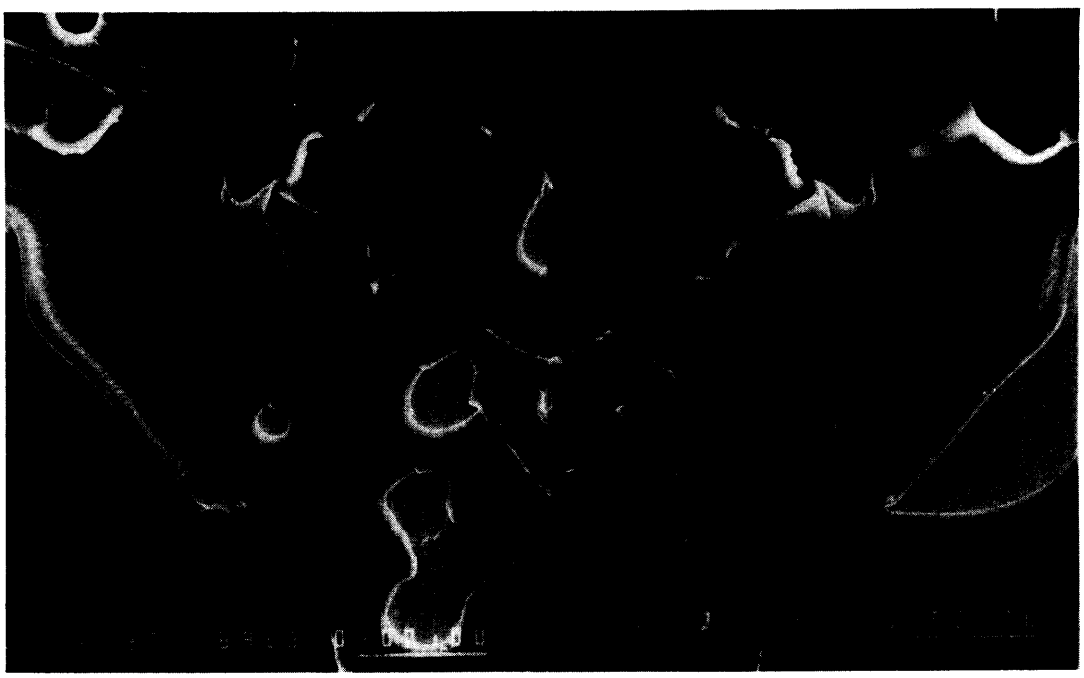

Fig. 11. A mated pair of in-layer fracture surfaces. The brighter patches are the metal surfaces where the metal/epoxy interface decohered. The darker portions are remaining epoxy after the in-layer fracture.

Fig. 12. A sequence of micrographs with increasing magnifications. (a) A mated pair of in-layer fracture surface at a low magnification. One can see a mixture of fractured epoxy layers and metal surfaces. (b) At a higher magnification such a mixture is shown at a more microscopic level. (c) At a still higher magnification, one can see micro-kinks.

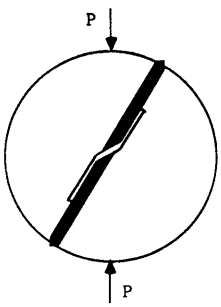

Fig. 13. A modified Brazil-nut-sandwich.

to be 1–40 μm. The interlayer thickness h was measured to be in the range 80–300 μm. We believe the small scale yielding condition is approximately satisfied in most of our tests.

5.2. Small scale contact

The requirement of small scale contact sets the range of the loading phase in which toughness can be validly measured for a given interface. Due to the peculiar singularity, equation (5) shows that $\delta_y < 0$ must occur for some sufficiently small r. Given a specimen with the K-calibration (10), with specimen size L and loading angle ψ, one deduces from (5) that

$$\delta_y = |\delta| \cos[\psi - \epsilon \ln(L/r) - \tan^{-1}(2\epsilon)] \quad (17)$$

where $|\delta|$ is the magnitude of the crack face displacement jump. For a valid test the small scale contact condition requires that $\delta_y > 0$ when $L/100 < r < L$ (the number 100 is chosen arbitrarily, but the absolute value of this number will not affect the following result significantly). This requirement confines the range of ψ in which valid toughness can be measured

$$-\pi/2 + 6.6\epsilon < \psi < \pi/2 + 2\epsilon, \quad \text{for } \epsilon > 0$$
$$-\pi/2 + 2\epsilon < \psi < \pi/2 + 6.6\epsilon, \quad \text{for } \epsilon < 0 \quad (18)$$

This in turn sets a limit to loading phase $\hat{\psi}$ [see equation (11)].

With sandwich specimens, we have chosen $\hat{L} = L = h$ in (11), so that $\hat{\psi} \approx \psi$. For steel/epoxy interface, for example, $\epsilon = -0.075$, which yields $-99° < \hat{\psi} < 61°$. In our experimental plots for metal/epoxy (Fig. 7), some data points are out of this validity range. Large contact is anticipated for these loading phases, which may account for the high apparent toughness compared with the trend set by the toughness values at lower loading phases.

5.3. Crack kinking out of an interface

Crack kinking out of an interface is studied recently in [17–19], where a criterion for a crack to favor kinking as opposed to running on the interfaces is proposed on the energetic basis. Consider a given pre-existing interfacial crack subjected to a certain loading phase $\hat{\psi}$. The crack is believed to kink when the fracture toughness ratio of the bulk material to the interface is less than the maximum value (over all potential kink angles) of the energy release rate ratio of a kinking crack to the interfacial crack. The latter ratio is obtained in [17] by solving an elasticity problem, and is about 1 for most material combinations under predominantly opening mode $\hat{\psi} \approx 0$.

This energetic criterion does not account for the kinking behavior observed in the present work. Toughness ratios of the bulk epoxy to the metal/epoxy interfaces at low loading phases exceed 5. However, kinking took place in most metal/epoxy disks when loaded remotely at mode I (compression angle $\theta = 0$). We propose an explanation for this experimental observation.

Consider an adhesive joint under remote mode I loading K_I^∞, with a primary interfacial crack and an initial kink-like flaw of size b at angle Ω to the interface, see Fig. 14. The following paragraph estimates the mode II stress intensity factor at the kink tip and the final result is equation (22).

The complex stress intensity factor of the interfacial crack in the sandwich structure in absence of the kink is [16]

$$K = (1-\alpha)^{1/2} \cosh(\pi\epsilon) K_I^\infty h^{-i\epsilon} e^{i\omega}. \quad (19)$$

Here ω is the same as that in Section 3.2, i.e. $\omega = -13°$ for the metal/epoxy systems. When the initial flaw is small, i.e. $b/h \ll 1$, the stress intensity factors at the kink tip can be estimated by the asymptotic solution in [17] with the complex interfacial K as

$$K_I = c_{11}\,\mathrm{Re}[Kb^{i\epsilon}] + c_{12}\,\mathrm{Im}(Kb^{i\epsilon}]$$
$$K_{II} = c_{21}\,\mathrm{Re}[Kb^{i\epsilon}] + c_{22}\,\mathrm{Im}(Kb^{i\epsilon}]. \quad (20)$$

Here c_{ij} are dimensionless numbers dependent on the elastic mismatch constants α and β and the kink angle Ω, and available in [18]. Values of c_{21} for three material combinations are cited in Table 3. Combining (19) and (20), one obtains

$$K_{II} = \cosh\ \pi\epsilon (1-\alpha)^{1/2} K_I^\infty \left\{ c_{21} \cos\left(\omega + \epsilon \ln \frac{b}{h}\right) + c_{22} \sin\left(\omega + \epsilon \ln \frac{b}{h}\right) \right\}. \quad (21)$$

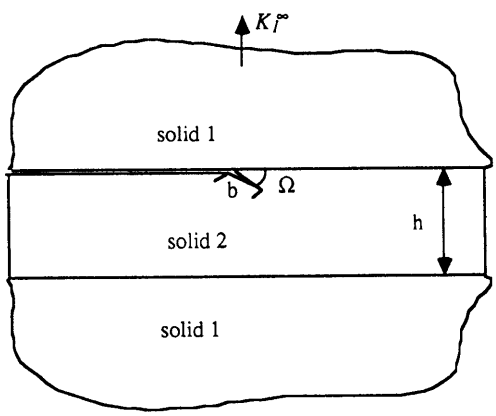

Fig. 14. Crack kinking in an adhesive joint.

With typical numbers for the metal/epoxy systems, $\omega = -13°$, $\alpha = 0.9$, $\epsilon = -0.07$, $b/h = 1/30$, equation (21) gives

$$K_{II} \approx 0.3 c_{21} K_I^{\infty}. \tag{22}$$

This last expression is insensitive to the value we assigned to b/h, as a result of the logarithmic dependence.

As indicated in Table 3, c_{21} is positive for large elastic mismatch for most kink angles. The implication is that, in seeking a local mode I trajectory, an initial kink-like flaw is encouraged by the positive local K_{II} to divert further away from the interface, even though the remote load is mode I. This fact results entirely from the large elastic mismatch. For comparison, c_{21} is negative in elastically homogeneous systems ($\alpha = \beta = 0$) at any kink angle, as indicated in Table 3.

It is clear the effect is not an artifact of the non-oscillatory index ϵ or the sandwich structure. However, it does require the presence of initial kink-like flaw near the interface. As an interfacial crack is under a predominantly opening mode, i.e. $\mathrm{Im}[Kb^{i\epsilon}] \approx 0$ and $\mathrm{Re}[Kb^{i\epsilon}] > 0$, it is seen from (20) that K_{II} at the kink tip is positive when c_{21} is. Consequently, interfacial cracks in bimaterials with large elastic mismatch have a strong tendency to kink under predominantly opening mode. Notice this assertion is independent of the toughness ratio of the bulk material to the interface, so long as this ratio is not too large to invalidate the linear fracture mechanics approach or to cause essentially no adhesion of the interface.

5.4. *In-layer fracture of adhesive joints*

If a flat crack is perfectly confined in the thin epoxy layer, owing to the conservation of the J-integral, the apparent toughness G_c calculated from the remote load is identical to the fracture energy of the bulk epoxy. Fractographs show that the fracture surface in type 5 failure consists of epoxy residue as well as patches of metal surfaces. What we measured in this case, as a consequence, was essentially an area average of the bulk epoxy fracture energy and metal/epoxy interfacial toughness. In our case, G_c ($> 50\, J\, m^{-2}$) for bulk epoxy is much higher than G_c for interfaces at $\theta \approx 0°$. The measured fracture energy (solid circles in Fig. 7) lies well within these two values, which confirms the above consideration. Large scattering of full circles reflects the uncertainty of the area fraction of the metal surface patches in our experiments.

An anomaly is that the crack favors a path within the layer with higher fracture resistance than the interfaces. An idealized problem that a flat crack perfectly confined in the layer is analyzed recently. The details are reported elsewhere [20], and here we only cite the major findings.

For a base specimen under remote mode I loading, the center plane parallel to the interfaces in the adhesive layer is locally mode I crack plane, as inferred by symmetry. A parallel crack plane off the center plane in the layer is not pure mode I. The sign of the local K_{II} depends on the elastic moduli mismatch, as well as the location of the plane. When the interlayer is compliant compared with the substrates, as for metal/epoxy systems, the sign of the K_{II} is found to encourage a crack off the center plane to divert into the center plane. A corollary is that when the pre-crack is not precisely on the interface, either due to the specific way we introduce the pre-crack or due to the flaw perturbation, it will be trapped to the center plane in the layer rather than divert back to the interface. Another finding in [20] is that the so-called T-stress is compressive in the layer around the crack tip when the layer is relatively compliant and the residual stress in the layer is not too large and tensile. This compressive stress in the crack direction stabilizes a mode I straight crack against small perturbations, as discussed in [21].

The in-layer stable crack path is primarily accommodated by large elastic mismatch between the substrates and adhesive layer, such as in metal/epoxy systems. Specifically, in-layer fracture is favorable as the layer material is more compliant than the substrates. We never found in-layer fracture in plexiglass/epoxy specimens, where the elastic modulus for the layer is relatively rigid. Consequently, the latter arrangement is more suitable to measure interfacial toughness.

Table 3. Values of c_{21}

Ω	10°	30°	50°	70°	90°
$\alpha = -0.75$, $\beta = -0.25$	0.62	0.58	0.54	0.47	0.38
$\alpha = 0$, $\beta = 0$	−0.09	−0.24	−0.34	−0.38	−0.35
$\alpha = 0.8$, $\beta = 0.45$	−0.15	0.08	0.27	0.34	0.32

6. SUMMARY OF RESULTS

We have developed a Brazil-nut-sandwich for interfacial fracture testing. The strategy is to use one single type of specimen to generate the full interfacial toughness curves, in contrast to earlier work [10] using a different specimen for each loading phase. A desirable feature of sandwiches is that the residual stress in the layer, which is inevitable in practice, does not drive cracks, and thus one does not have to independently measure the residual stress to obtain interfacial toughness. A modified Brazil-nut-sandwich is proposed (without testing) allowing more rigorous data conversion. The microscopic failure behaviors pose several paradoxes and are explained on the basis of several recent elasticity solutions. We found, experimentally and theoretically, there is an inherent tendency for an interfacial crack to kink into an adjacent solid even though it is energetically unfavorable.

Acknowledgements—We thank J. W. Hutchinson, J. R. Rice and C. F. Shih for helpful discussions. Support was provided at Harvard University through sub-agreement

VB38639-0 with the University of California at Santa Barbara, based on the Office of Naval Research contract N00014-86-K-0753, and for JSW through a visiting scholar program at Max-Planck Institut, for ZS through a new faculty funding at the University of California, Santa Barbara.

REFERENCES

1. J. R. Rice, *J. appl. Mech* **55,** 98 (1988).
2. J. W. Hutchinson, *Scripta metall.* In press.
3. C. F. Shih, R. J. Asaro and N. P. O'Dowd, *Scripta metall.* In press.
4. A. G. Evans, M. Ruhle, B. J. Dalgleish and P. G. Charalambides, *Scripta metall.* In press.
5. J. R. Rice, Z. Suo and J. S. Wang, *Scripta metall.* In press.
6. Z. Suo, Ph.D. thesis, Harvard Univ. (1989).
7. M. S. Hu and A. G. Evans, *Acta metall.* **36,** 1301 (1988).
8. Z. Suo and J. W. Hutchinson, *Int. J. Solids Struct.* **25,** 1337 (1989).
9. Z. Suo and J. W. Hutchinson, *Int. J. Fract.* In press.
10. H. C. Cao and A. G. Evans, *Mech. Mater.* **7,** 295 (1989).
11. A. G. Evans and J. W. Hutchinson, *Acta metall.* **37,** 909 (1989).
12. J. Dundurs, *J. appl. Mech.* **36,** 650 (1969).
13. M. L. Williams, *Bull. Seismol. Soc. Am.* **49,** 199 (1959).
14. C. Atkinson, R. E. Smelser and J. Sanchez, *Int. J. Fract.* **18,** 279 (1982).
15. D. Singh and D. K. Shetty, *J. Am. Ceram. Soc.* **72,** 78 (1989).
16. Z. Suo and J. W. Hutchinson, *Mater. Sci. Engng* **A107,** 135 (1989).
17. M.-Y. He and J. W. Hutchinson, *J. appl. Mech.* **56,** 270 (1989).
18. M.-Y. He and J. W. Hutchinson, Harvard Univ. Report, MECH-113A.
19. A. G. Evans, B. J. Dalgleish, M.-Y. He and J. W. Hutchinson. To be published.
20. N. A. Fleck, J. W. Hutchinson and Z. Suo, Harvard Univ. Report, MECH-156.
21. B. Cotterell and J. R. Rice, *Int. J. Fract.* **16,** 155 (1980).